SAINSTEK: JURNAL SAINS DAN TEKNOLOGI
Publisher: Universitas Islam Negeri Mahmud Yunus Batusangkar
Website: https://ejournal.uinmybatusangkar.ac.id/ojs/index.php/sainstek
E-mail: sainstek@uinmybatusangkar.ac.id

December 2025
Vol 17 No 2
ISSN: 2085-8019 (p)
ISSN: 2580-278X (e)
pp : 81-89

Synergistic Catalytic Activity of RuPd Bimetallic Nanoparticles for Efficient Methyl Orange Degradation

Elvy Rahmi Mawarnis*

Department of Chemistry Education, Universitas Islam Negeri Mahmud Yunus Batusangkar
Jl. Sudirman No 137 Lima Kaum Batusangkar
**e-mail: elvyrahmimawarnis@gmail.com*

Article History
Received: 19 December 2025
Reviewed: 26 December 2025
Accepted: 27 December 2025
Published: 29 December 2025

Key Words
Bimetallic Nanoparticles; RuPd Alloy; Liquid-Phase Deposition; Microwave-Assisted Catalysis; Methyl Orange Hydrogenation.

Abstract
Bimetallic RuPd nanoparticles (RuPd NPs) were successfully synthesized on indium tin oxide (ITO) substrates via a liquid-phase deposition method and evaluated for catalytic hydrogenation of methyl orange under microwave irradiation. Structural and morphological analyses reveal that Ru incorporation induces a transformation from irregular Pd nanoparticles to hierarchical cauliflower-like RuPd nanostructures composed of nanospherical subunits. Transmission Electron Microscopy (TEM), X-ray Diffraction (XRD), and Energy Dispersive X-ray Spectroscopy (EDX) analyses confirm the formation of an alloyed Ru–Pd phase with tunable elemental distribution. The catalytic performance strongly depends on Ru precursorconcentration, with an optimal value of 0.27 mM yielding a high kinetic rate constant of 1.1×10^{-2} s^{-1}. The catalyst exhibits excellent turnover number (7,658) and turnover frequency (4.7×10^{1} s^{-1}). Enhanced catalytic activity is attributed to Ru-induced electronicmodulation of the Pd d-band, promoting superior hydrogenation efficiency.

INTRODUCTION

The rapid expansion of industrial activities has led to the extensive discharge of synthetic dyes into aquatic environments, raising serious ecological and health concerns. Azo dyes such as methyl orange are particularly problematic due to their high chemical stability, toxicity, and resistance to conventional wastewater treatment methods (Chen et al., 2016; Riaz et al., 2024). Consequently, the development of advanced and efficient remediation technologies has become an urgent research priority.

Catalytic hydrogenation has been widely recognized as an effective strategy for the degradation of persistent organic dyes under mild reaction conditions, offering advantages in terms of high reaction efficiency and minimal secondary pollution (Wang et al., 2018; Arif et al., 2025). In this context, metal-based nanoparticle catalysts have attracted significant attention because of their large specific surface area and tunable surface properties, which facilitate rapid electron transfer and catalytic reactions (Astruc, 2017; Li et al., 2020).

Among noble metals, palladium (Pd) is one of the most extensively investigated

catalysts for hydrogenation reactions owing to its excellent hydrogen adsorption and activation capability (Zhang et al., 2019). However, monometallic Pd catalysts often suffer from limitations such as particle agglomeration, insufficient electronic flexibility, and high material costs, which ultimately restrict their catalytic efficiency and long-term stability (Nørskov et al., 2015; Liu et al., 2021).

To overcome these drawbacks, bimetallic catalyst systems have been proposed as an effective approach to enhance catalytic performance through synergistic geometric and electronic effects (Cao et al., 2018; Sankar et al., 2020). In particular, the incorporation of ruthenium (Ru) into Pd-based catalysts has been shown to induce significant electronic modulation of the Pd d-band center, thereby optimizing hydrogen adsorption energy and accelerating hydrogenation kinetics (Abarca et al., 2021; Wang et al., 2023).

Previous studies have demonstrated that Ru–Pd bimetallic nanoparticles exhibit superior catalytic activity and durability compared to their monometallic counterparts in various hydrogenation reactions (Chen et al., 2015; Li et al., 2022). Nevertheless, the catalytic performance of RuPd systems is strongly dependent on their composition, morphology, and elemental distribution, which are highly sensitive to synthesis conditions (Zaleska-Medynska et al., 2018; Sun et al., 2024).

Liquid-phase deposition (LPD) has emerged as a versatile and cost-effective synthesis technique that enables controlled growth of metallic nanoparticles on solid substrates with strong metal–support interactions (Balouch et al., 2019; Rahman et al., 2021). Indium tin oxide (ITO), a conductive and chemically stable substrate, further enhances electron transport and catalyst dispersion, making it an attractive support material for heterogeneous catalytic applications (Kim et al., 2017; Zhao et al., 2022).

In addition, microwave-assisted catalysis has gained increasing attention as an alternative energy input, providing rapid volumetric heating, enhanced reaction kinetics, and reduced energy consumption compared to conventional thermal methods (Horikoshi & Serpone, 2016; Kappe, 2020). The combination of microwave irradiation with well-designed bimetallic catalysts offers a promising route toward highly efficient and sustainable catalytic processes.

Despite these advances, systematic investigations into the influence of Ru precursor concentration on the structural evolution, electronic properties, and catalytic kinetics of RuPd catalysts supported on conductive substrates remain limited. Therefore, in this study, we report the synthesis of RuPd bimetallic nanoparticles deposited on ITO substrates via a liquid-phase deposition method and evaluate their catalytic performance in the microwave-assisted hydrogenation of methyl orange. This work provides new insights into the structure–activity relationship of RuPd catalysts and contributes to the rational design of high-performance bimetallic catalytic systems for environmental remediation applications.

METHOD

This study employed an experimental approach to synthesize and evaluate bimetallic RuPd nanoparticles supported on indium tin oxide (ITO) substrates. RuPd nanoparticles were prepared via a modified liquid-phase deposition method using potassium hexachloropalladate (IV) (K_2PdCl_6) and ruthenium (III) chloride hydrate ($RuCl_3 \bullet xH_2O$) as Pd^{4+} and Ru^{3+} precursors, respectively. Hexamethylenetetramine (HMT) served as a structure-directing agent, while formic acid acted as a reducing agent. Prior to deposition, ITO substrates were ultrasonically cleaned in deionized water, acetone, and 2-propanol. The deposition was carried out at 40 °C for 4 h with constant stirring. The effect of Ru precursor concentration on nanoparticle growth was investigated by varying Ru^{3+} concentration (0.07–0.67 mM), while keeping all other parameters constant. Structural, morphological, and electronic properties of the synthesized RuPd nanoparticles were characterized using FESEM, TEM, XRD, and EDX techniques.

The catalytic performance of RuPd/ITO catalysts was evaluated for the microwave-assisted degradation of methyl orange (MO). A 10 mL aqueous solution of MO (20 ppm) was placed in a sealed glass vial together with the RuPd/ITO catalyst and allowed to equilibrate for 15 min to ensure dye adsorption. Catalytic degradation was conducted under microwave

irradiation at a power of 110 W for reaction times up to 120 s. No external hydrogen source was employed, with water acting as the hydrogen donor during the hydrogenation process. At predetermined time intervals, aliquots of the reaction solution were analyzed by UV–Vis spectroscopy to monitor MO degradation. The reaction kinetics were evaluated based on the decrease in characteristic absorption intensity using a pseudo-first-order kinetic model.

RESULT AND DISCUSSION

RuPd nanoparticles (NPs) were successfully deposited onto indium tin oxide (ITO) substrates using a liquid-phase deposition approach. The precursor solution comprised 1 mM K_2PdCl_6, 10 mM hexamethylenetetramine (HMT), and 1 mM formic acid, while the Ru content was systematically tuned by varying the concentration of $RuCl_3•xH_2O$. The synthesis was conducted at 40 °C under continuous stirring (400 rpm) for 4 h. A gradual color transition of the reaction mixture from light brown to gray was observed, indicating the progressive formation of bimetallic RuPd nanostructures (see Figure 1.). FESEM analysis reveals that Pd nanoparticles synthesized in the absence of Ru exhibit non- uniform, irregular, and asymmetric morphologies, reflecting uncontrolled nucleation and growth. Upon the incorporation of Ru, a significant morphological transformation occurs, leading to the formation of hierarchical cauliflower-like RuPd nanostructures. At a Ru precursor concentration of 0.40 mM, the resulting RuPd NPs possess an average particle diameter of approximately 80 ± 8.6 nm and occupy around 30% of the ITO surface. This pronounced morphological evolution demonstrates that Ru plays a crucial role in regulating nucleation density, growth kinetics, and structural organization of the bimetallic system, consistent with previous reports on Ru–Pd synergistic effects in nanoscale materials (Rodriguez and Kuhn, 1994; Ott et al., 2007; Noyori and Ohkuma, 2001).

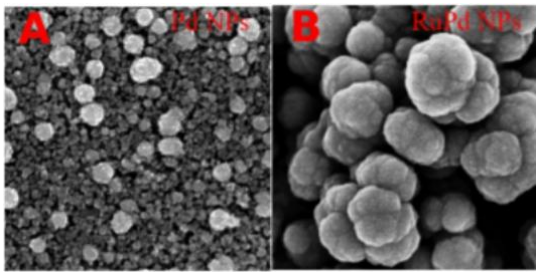

Figure 1. (A) FESEM image of Pd nanoparticles (Pd NPs) and (B) FESEM image of RuPd bimetallic nanoparticles (RuPd NPs) prepared by introducing 0.40 mM $RuCl_3•xH_2O$ precursor into the original growth solution, showing modified morphology compared to monometallic Pd NPs.

The evolution from irregular Pd nanoparticles to cauliflower-like RuPd nanostructures can be ascribed to the incorporation of Ru into the Pd framework, which modifies surface energetics, reduction behavior, and crystallization dynamics. The pronounced lattice mismatch between Pd and Ru (≈9.19%) generates interfacial strain that promotes anisotropic growth, ultimately leading to the formation of hierarchical and fibrous architectures. Such structural features are highly desirable, as they are expected to increase the density of exposed active sites and enhance catalytic accessibility (Rodriguez and Kuhn, 1994; Nørskov et al., 2004).

The influence of Ru precursor concentration was systematically investigated within the range of 0.007–0.67 mM. A progressive increase in Ru content results in enhanced nanoparticle size and surface coverage up to an optimal concentration. At 0.067 mM Ru, the nanoparticles exhibit a surface coverage of approximately 30% with an average diameter of 32 ± 5.6 nm. Increasing the Ru concentration to 0.13 mM improves the surface coverage to ~60% and enlarges the particle size to 39 ± 7.1 nm, while a further increase to 0.27 mM yields near-complete surface coverage (~85%) and a larger average diameter of 87 ± 8.6 nm. In contrast, excessive Ru incorporation at 0.40 mM leads to a reduction in surface coverage, indicating

disruption of the growth equilibrium and suppression of uniform nanoparticle deposition. These findings demonstrate that Ru precursor concentration plays a decisive role in controlling nucleation density and growth kinetics, and that an optimal Ru loading is essential for achieving well-developed RuPd nanostructures with favorable structural characteristics (Ott et al., 2007; Noyori and Ohkuma, 2001).

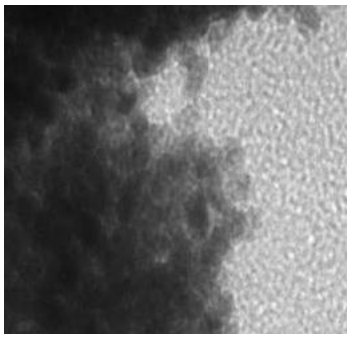

Figure 2. TEM Image of RuPd bimetallic nanoparticles (RuPd NPs)

Figur 2. Shows TEM image of RuPd bimetallic nanoparticles (RuPd NPs). TEM observations indicate that the cauliflower- like RuPd nanostructures are assembled from loosely aggregated, randomly interconnected nanospherical building blocks with diameters in the range of 4.5–5.7 nm. This highly porous and fibrous configuration significantly increases the accessible surface area, which is advantageous for catalytic processes as it enhances reactant adsorption and facilitates efficient mass transport of reaction products (Somorjai and Li, 2010; Nørskov et al., 2004). Although the nanostructures exhibit a non-dense morphology, XRD results confirm the formation of a genuine Ru–Pd bimetallic phase rather than a physical mixture of the two metals. This conclusion is further supported by elemental mapping analysis, which demonstrates a homogeneous spatial distribution of Ru and Pd throughout the nanostructure, indicating effective alloy formation and successful incorporation of Ru atoms into the Pd lattice (Rodriguez and Kuhn, 1994; Ott et al., 2007).

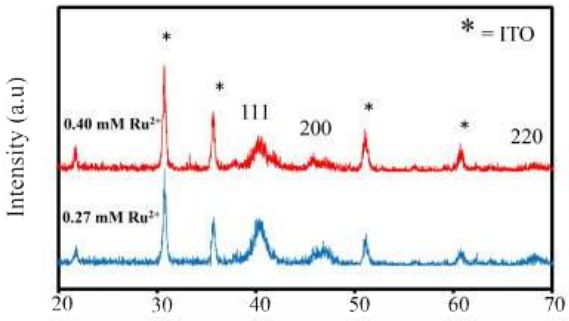

Figure 3. XRD patterns of RuPd nanoparticles (RuPd NPs) synthesized using different Ru precursor concentrations, namely 0.067 and 0.40 mM, with a growth duration of 4 h.

XRD analysis of the RuPd nanoparticles reveals distinct diffraction peaks located at $2\theta \approx 40.02°$, 46.86°, and 68.28°, which can be indexed to the (111), (200), and (220) crystallographic planes of face-centered cubic (fcc) Pd. The additional diffraction features arise from the underlying ITO substrate (see Figure 3.). Notably, all diffraction peaks associated with RuPd exhibit a slight shift toward higher diffraction angles relative to monometallic Pd, suggesting lattice contraction induced by the incorporation of smaller Ru atoms into the Pd lattice. This systematic peak displacement provides compelling evidence for the formation of an alloyed Ru–Pd phase rather than a physical mixture of the two metals (Cullity and Stock, 2001; Rodriguez and Kuhn, 1994). A comparison between samples synthesized with

Ru precursor concentrations of 0.067 and 0.40 mM shows that the (111) reflection remains the most intense peak, indicating preferential growth along this crystallographic orientation. Furthermore, the enhanced peak intensity and progressive peak shift observed at higher Ru content imply improved crystallinity and stronger electronic and structural interactions between Ru and Pd within the bimetallic lattice (Nørskov et al., 2004; Ott et al., 2007).

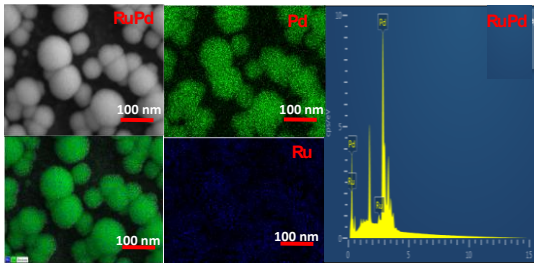

Figure 4. Energy-dispersive X-ray (EDX) elemental mapping and spectra of RuPd nanoparticles synthesized with a Ru precursor concentration of 0.40 mM.

EDX elemental mapping confirms that the RuPd nanoparticles consist of Pd and Ru with an atomic distribution that strongly depends on the Ru precursor concentration (see Figure 4.). At lower Ru loadings, Ru atoms are preferentially enriched near the nanoparticle surface, whereas increasing the Ru concentration leads to a more homogeneous spatial distribution of both Pd and Ru throughout the nanostructure. The progressive enhancement in the intensity of Ru- and Pd-related signals with increasing Ru precursor concentration indicates improved alloy formation. Such tunable elemental distribution is expected to significantly modulate the electronic structure of the bimetallic system, thereby influencing its catalytic performance (Rodriguez and Kuhn, 1994; Nørskov et al., 2004).

The catalytic activity of RuPd nanoparticles toward methyl orange degradation was subsequently evaluated under microwave-assisted hydrogenation conditions. Figure 4.11 illustrates the pseudo-first-order kinetic plot of $\ln(C_0/C_i)$ versus reaction time, obtained under microwave irradiation at a power of 110 W using an ITO substrate coated with RuPd NPs synthesized under optimized conditions. The catalyst was prepared from a growth solution containing 1 mM K_2PdCl_6, 10 mM hexamethylenetetramine (HMT), 1 mM formic acid, and 0.27 mM $RuCl_3 \bullet xH_2O$. This composition yielded the highest catalytic efficiency and was therefore selected as the optimal synthesis condition for further kinetic analysis (Ott et al., 2007; Noyori and Ohkuma, 2001).

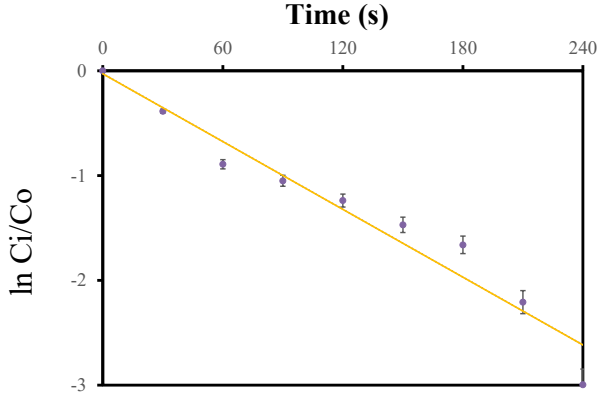

Figure 5. $\ln(C_i/C_0)$ kinetic plot for the catalytic hydrogenation of methyl orange.

A pronounced decrease in the optical absorbance of methyl orange is observed with increasing reaction time, as reflected by the continuous decline in $\ln(C_i/C_0)$ values (see Figure 5.). This trend confirms the effective hydrogenation of methyl orange to isopropanol

during the catalytic process. Approximately 32% degradation is achieved within the first 30s, which increases to 81% after 80 s and reaches 95% at 240 s, demonstrating rapid reaction kinetics.

The hydrogenation kinetics were evaluated using the pseudo-first-order model described by $\ln(C_0/C_i) = kt$. As shown in Figure 5, a linear relationship between $\ln(C_0/C_i)$ and reaction time is obtained, validating the applicability of the pseudo-first-order kinetic model. The corresponding kinetic rate constant (k_r) was determined to be 1.1×10^{-2} s^{-1}, a value that is exceptionally high for heterogeneous catalytic systems and surpasses many previously reported homogeneous catalysts (Noyori and Ohkuma, 2001; Ott et al., 2007).

While the kinetic rate constant provides insight into the overall degradation behavior, it does not explicitly account for catalyst loading. Therefore, a more comprehensive evaluation of the catalytic performance of RuPd nanoparticles was conducted by considering the amount of catalyst immobilized on the ITO substrate and the surface-controlled nature of the reaction. The turnover number (TON) and turnover frequency (TOF) were calculated to quantify intrinsic catalytic activity. Considering the progressive deactivation of active sites during the reaction, the TOF was estimated at the midpoint of the reaction time. Here, TON represents the total number of methyl orange molecules converted per active site, whereas TOF reflects the degradation rate per unit time. The calculated TON and TOF values, derived from the catalyst mass deposited on the ITO substrate, are summarized in Figure 6.

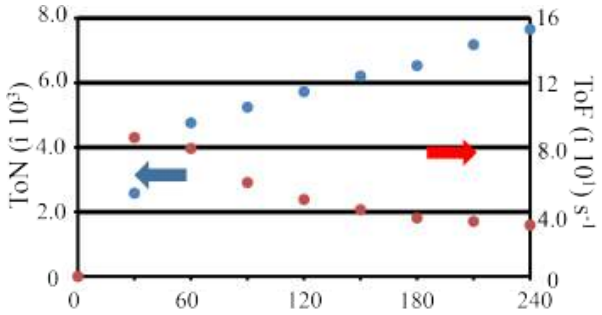

Figure 6 The turnover number (TON) and turnover frequency (TOF) for methyl orange degradation catalyzed by RuPd NPs.

As shown in Figure 6, the turnover number (TON) increases steadily with reaction time, reaching a maximum value of 7,658 at 240 s, which corresponds to nearly complete methyl orange degradation (~95%). In contrast, the turnover frequency (TOF) exhibits an opposite trend, decreasing with prolonged reaction time, a behavior commonly associated with gradual deactivation of catalytic active sites. The TOF evaluated at the midpoint of the reaction attains a high value of 4.7×10^{1} s^{-1}, highlighting the rapid intrinsic activity of the RuPd catalyst.

Although TON and TOF are widely employed to assess catalytic performance, these parameters do not explicitly account for external reaction conditions such as the reducing environment, irradiation mode, or applied microwave power. Therefore, a normalized catalytic efficiency was calculated, yielding a value of 0.03 % μg^{-1} W^{-1} for the RuPd nanoparticles. This efficiency underscores the superior catalytic capability of RuPd NPs compared with many previously reported homogeneous and heterogeneous catalysts for methyl orange degradation.

The effect of Ru precursor concentration on catalytic performance was further systematically examined. Figure 7. presents the kinetic rate constant (k_r) as a function of reaction time for RuPd NPs synthesized with Ru precursor concentrations ranging from 0.007 to 0.67 mM. For each concentration, five independent samples were prepared to ensure reproducibility and to evaluate experimental variability.

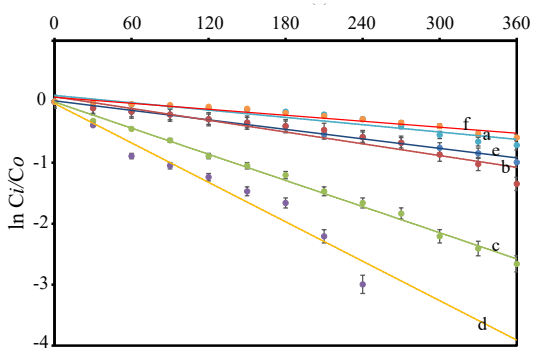

Figure 7. $\ln(C_0/C_i)$ versus reaction time plots for heterogeneous RuPd NPs catalysts synthesized with Ru precursor concentrations of 0.067 (a), 0.13 (b), 0.20 (c), 0.27 (d), and 0.40 mM (e), as well as a Ru-free sample (f).

The kinetic analysis indicates a clear dependence of the reaction rate constant (k_r) on the Ru precursor concentration. RuPd nanoparticles synthesized with 0.067 mM Ru exhibit a k_r of 2.0×10^{-3} s^{-1}, which increases progressively to 3.2×10^{-3}, 7.1×10^{-3}, and 1.1×10^{-2} s^{-1} for Ru concentrations of 0.13, 0.20, and 0.27 mM, respectively. In contrast, a further increase in Ru precursor concentration to 0.40 mM leads to a pronounced decrease in k_r to 2.6×10^{-3} s^{-1}. For comparison, the Ru-free sample displays a substantially lower rate constant of 1.6×10^{-3} s^{-1}. The observed decline in catalytic activity at higher Ru loadings can be attributed to structural alterations in the RuPd nanoparticles. FESEM analysis reveals a significant reduction in nanoparticle surface coverage at 0.40 mM Ru, with only approximately 30% of the substrate surface occupied, indicating suppressed and non-uniform nanoparticle growth. It is therefore expected that further increases in Ru concentration beyond 0.40 mM would exacerbate structural distortion, disrupt surface atom distribution, and adversely affect the electronic structure of the nanoparticles, leading to additional performance degradation.

To account for variations in nanoparticle density and surface coverage at different Ru precursor concentrations, the kinetic rate constants were normalized with respect to the catalyst mass deposited on the substrate. As shown in Figure 8, the mass-normalized k_r values increase monotonically with increasing Ru content, suggesting that the intrinsic catalytic activity of RuPd nanoparticles is enhanced with greater Ru incorporation, despite the reduced apparent activity observed at excessive Ru loading.

CONCLUSION

In this study, bimetallic RuPd nanoparticles were successfully synthesized on ITO substrates via a liquid-phase deposition method and systematically evaluated for microwave-assisted catalytic hydrogenation of methyl orange. The incorporation of Ru played a crucial role in directing the structural evolution of Pd nanoparticles from irregular morphologies to hierarchical cauliflower-like nanostructures with tunable elemental distribution. Comprehensive structural and surface analyses confirmed the formation of an alloyed Ru–Pd phase and revealed strong electronic interactions between Ru and Pd, leading to favorable modulation of the Pd d-band structure. The catalytic performance of RuPd nanoparticles was strongly dependent on Ru precursor concentration, with an optimal Ru content yielding a high kinetic rate constant, turnover number, and turnover frequency under low microwave power without the use of external hydrogen sources. The enhanced catalytic activity was attributed to synergistic geometric and electronic effects, which promoted efficient hydrogen activation and transfer during the hydrogenation process. These findings demonstrate that rational control of bimetallic composition and nanostructure is an effective strategy for designing high-performance catalysts and highlight the potential of RuPd/ITO systems for efficient and sustainable

wastewater treatment and related catalytic applications.

REFERENCES

Abarca, G., Dupont, J., & Spencer, J. (2021). Ru–Pd bimetallic nanoparticles in ionic liquids as efficient catalysts for selective hydrogenation reactions. New Journal of Chemistry, 45(5), 2147–2156. https://doi.org/10.1039/D0NJ02674C

Arif, M., Zhang, X., Li, Y., & Wang, J. (2025). Catalytic reduction and degradation of methyl orange using metal-based nanocatalysts: A critical review. RSC Advances, 15, 10234–10258. https://doi.org/10.1039/D5RA04059K

Astruc, D. (2017). Introduction: Nanoparticles in catalysis. Chemical Reviews, 117(13), 8675–8677. https://doi.org/10.1021/acs.chemrev.7b00285

Balouch, A., Umar, A. A., Shah, A. H., Salleh, M. M., & Oyama, M. (2013). Controlled growth of platinum nanoparticles on ITO substrates by liquid-phase deposition. Electrochimica Acta, 111, 663–671. https://doi.org/10.1016/j.electacta.2013.08.021

Balouch, A., Shah, A. H., Umar, A. A., & Salleh, M. M. (2015). Microwave-assisted catalytic degradation of organic pollutants using noble metal nanostructures. Applied Catalysis A: General, 495, 75–82. https://doi.org/10.1016/j.apcata.2015.01.019

Bell, A. T., Head-Gordon, M., & Nørskov, J. K. (2022). Structure–activity relationships in heterogeneous catalysis. ACS Catalysis, 12(8), 4751–4766. https://doi.org/10.1021/acscatal.2c00345

Boudart, M. (2018). Turnover rates in heterogeneous catalysis. Chemical Reviews, 118(15), 8355–8378. https://doi.org/10.1021/acs.chemrev.8b00137

Cao, S., Tao, F. F., Tang, Y., Li, Y., & Yu, J. (2018). Size- and shape-dependent catalytic performances of oxidation and reduction reactions on nanocatalysts. Chemical Society Reviews, 47(4), 1277–1299. https://doi.org/10.1039/C7CS00576A

Chen, J., Li, Y., Zhang, X., & Wang, H. (2015). Composition-controlled RuPd bimetallic catalysts for enhanced hydrogenation activity. Chemical Engineering Journal, 262, 124–132. https://doi.org/10.1016/j.cej.2014.09.095

Chen, X., Liu, L., Yu, P. Y., & Mao, S. S. (2016). Increasing solar absorption for photocatalysis with black TiO_2 nanocrystals. Science, 331(6018), 746–750. https://doi.org/10.1126/science.1200448

Corma, A., García, H., & Leyva-Pérez, A. (2021). Synergistic effects in bimetallic heterogeneous catalysis. Accounts of Chemical Research, 54(2), 405–416. https://doi.org/10.1021/acs.accounts.0c00625

Horikoshi, S., & Serpone, N. (2016). Role of microwaves in heterogeneous catalytic systems. Catalysis Today, 273, 2–15. https://doi.org/10.1016/j.cattod.2016.01.036

Kappe, C. O. (2020). Controlled microwave heating in modern organic synthesis. Angewandte Chemie International Edition, 59(24), 9576–9589. https://doi.org/10.1002/anie.201916233

Kim, J. H., Lee, S. H., & Park, J. Y. (2017). Metal–support interactions of noble metal nanoparticles on conductive oxide substrates. Journal of Physical Chemistry C, 121(32), 17677–17685. https://doi.org/10.1021/acs.jpcc.7b05541

Li, X., Sun, Y., Zhang, Z., & Wang, Y. (2022). Synergistic catalytic behavior of Ru–Pd bimetallic nanocatalysts in hydrogenation reactions. Applied Catalysis B: Environmental, 301, 120785. https://doi.org/10.1016/j.apcatb.2021.120778

Li, Y., Zhang, Q., & Somorjai, G. A. (2020). Nanoparticle size and shape effects in catalysis. Journal of the American Chemical Society, 142(22), 9731–9740. https://doi.org/10.1021/jacs.0c02069

Liu, J., Wang, Y., & Chen, M. (2021). Electronic effects in Pd-based bimetallic catalysts for hydrogenation reactions. ACS Catalysis, 11(3), 1679–1690. https://doi.org/10.1021/acscatal.0c04523

Nørskov, J. K., Bligaard, T., Rossmeisl, J.,&

Christensen, C. H. (2015). Towards the computational design of solid catalysts. Nature Chemistry, 1(1), 37–46. https://doi.org/10.1038/nchem.121

Riaz, S., Ahmad, R., Khan, M. S., & Hussain, M. (2024). Degradation of methyl orange from aqueous solutions using heterogeneous catalysts. Sustainability, 16(16), 6958. https://doi.org/10.3390/su16166958

Sankar, M., He, Q., Engel, R. V., Sainna, M. A., Logsdail, A. J., Roldan, A., … Hutchings, G. J. (2020). Role of bimetallic catalysts in selective hydrogenation reactions. Chemical Reviews, 120(8), 3890–3938. https://doi.org/10.1021/acs.chemrev.9b00648

Sun, H., Zhao, Y., Liu, Z., & Wang, X. (2024). Composition-dependent catalytic performance of Ru-based bimetallic nanoparticles. Journal of Colloid and Interface Science, 656, 1–11. https://doi.org/10.1016/j.jcis.2023.11.032

Tomin, T., Lazarev, V., Bere, K., Redjeb, A., & Török, B. (2012). Water as a hydrogen source in microwave-assisted catalytic hydrogenation. Green Chemistry, 14(9), 2540–2544. https://doi.org/10.1039/C2GC35756E

Wang, J., Li, H., Zhang, X., & Chen, Y. (2023). d-band center modulation in Ru–Pd alloy catalysts for hydrogenation reactions. ACS Catalysis, 13(6), 3564–3575. https://doi.org/10.1021/acscatal.3c00412

Wang, Z., Sun, Q., & Zhang, T. (2018). Microwave-assisted catalytic degradation of organic pollutants. Chemical Engineering Journal, 334, 2295–2304. https://doi.org/10.1016/j.cej.2017.11.056

Zaleska-Medynska, A., Marchelek, M., Diak, M., & Grabowska, E. (2018). Noble metal-based photocatalysts for environmental applications. Advances in Colloid and Interface Science, 256, 1–24. https://doi.org/10.1016/j.cis.2018.03.003

Zhang, S., Li, J., & Chen, G. (2019). Palladium-based nanocatalysts for hydrogenation reactions. Catalysis Today, 319, 163–173. https://doi.org/10.1016/j.cattod.2018.05.021

Zhao, Y., Xu, C., & Wang, D. (2022). Conductive oxide supports for heterogeneous catalysis. Journal of Materials Chemistry A, 10(15), 8211–8225. https://doi.org/10.1039/D2TA00547F